Solar Energy 187 (2019) 108–114

Contents lists available at ScienceDirect

Solar Energy

journal homepage: www.elsevier.com/locate/solener

New pyridyl-based dyes for co-sensitization in dye sensitized solar cells

Vanessa A. El Bitar Nehme, Melissa A. El Bitar Nehme, Tarek H. Ghaddar*

Department of Chemistry, American University of Beirut, Beirut 11-0236, Lebanon

ARTICLE INFO

Keywords:
DSSC
Solar cell
Impedance spectroscopy
Co-adsorption
Co-sensitization

ABSTRACT

Co-sensitization is very advantageous in increasing a dye sensitized solar cell's (DSSC) efficiency. It relies on sensitizing the same titania film with two dyes that have complementary absorption spectra. In this report we describe co-sensitization of dyes with pyridine anchoring groups with carboxylic-acid based ones having complementary absorption spectra. Six new pyridine based dyes with colors ranging from yellow to turquoise have been synthesized and characterized. T220, a yellow dye, was co-sensitized with Dyenamo Blue, a commercially available blue dye. This approach showed good performance enhancement compared to individual dye sensitized cells with a Co(II/III) redox mediator. An increase in the photocurrent (J_{SC}), photo-voltage (V_{oc}) and thus total efficiency (PCE%) were seen. The close packing of the two dyes in the co-sensitized devise caused a decrease in the electron recombination processes at the TiO_2/electrolyte interface, thus resulting in higher V_{oc} values. Such an increase in dye coverage results in a blocking behavior at the TiO_2/electrolyte interface, as mirrored in the performed electrochemical impedance spectroscopy (EIS) experiments, where higher charge recombination resistance (R_{CT}) and longer electron lifetime were measured in the co-sensitized DSSCs.

1. Introduction

Since 1991 upon the introduction of the well-known dye sensitized solar cell (DSSC) by O'Regan and Grätzel (1991) many research groups worked on increasing the DSSC efficiency using different methods for optimizing dyes' structures, electrolyte systems, electroactive material for counter electrode, etc… Record efficiencies (~15%) have been attained recently especially when using organic based dyes (Kakiage et al., 2015; Mathew et al., 2014; Yella et al., 2011). In the past couple of years, the research in the DSSC field has been focused on its indoor use at low-light conditions (Freitag et al., 2017; Tsai et al., 2018), and taking advantage of its aesthetic properties (Yun et al., 2015).

Co-sensitization in a DSSC involves the use of two different dyes that have complementary absorption spectra in order to maximize the light-harvesting efficiency of a DSSC across the whole visible light region (Hao et al., 2016; Islam et al., 2016; Kakiage et al., 2015; Kuang et al., 2007; Lodermeyer et al., 2016). In fact, one of the highest reported PCE % of 28.9% is for a co-sensitized DSSC under ambient lighting was attained by Freitag et al. (2017). Generally, upon successful co-sensitization higher photocurrents and a "maximized" incident-to-photon current conversion (IPCE%) are attained. However, most of the reported co-sensitization experiments in the literature are performed with two or more dyes having each a carboxylic acid anchoring group. Such anchoring groups bind preferentially to Brønsted-acid sites on TiO_2, which results in competition between these dyes to adsorb on the same sites of the semi-conductor. As such, the total dye loading in a co-sensitized DSSC would be less than the sum of the adsorbed amounts of the single-dye sensitized DSSCs (Hao et al., 2016; Islam et al., 2016; Yum et al., 2007). Recently, we reported on the co-sensitization of an organic dye, T181, with a pyridine moiety as an anchoring group with the carboxylic acid-based dye, Dyenamo Blue (Hao et al., 2016), while using a cobalt(II/III) tris-bipyridine electrolyte system (Hilal et al., 2018). Due to the fact that pyridine binds preferentially to the Lewis acid sites of TiO_2 (Harima et al., 2013), the total dye loading in a co-sensitized T181-DB film contained the same amounts of the two dyes as in the single dye-sensitized films. This clearly showed that dyes with different anchoring groups (such as pyridine and carboxylic acid in our case) would adsorb on different sites on TiO_2 and thus maximize the total dye loading.

In this work, we report the design, synthesis and characterization of six new organic dyes, T200 T201 T202 T220 T221 and T222, Scheme 1, having the form donor-π-acceptor-π-pyridine where all dyes are based on a pyridine anchoring group, a thiophene π bridge, and a bulky triphenylamine donor group which is verified to be favorable with cobalt redox electrolyte and results in lower recombination processes (Ellis et al., 2013). The middle acceptor group is varied among the six dyes in a way to obtain different colored dyes that span most of the visible absorption region (from 400 to 700 nm) (Joshi et al., 2018). This was

* Corresponding author.
E-mail address: tarek.ghaddar@aub.edu.lb (T.H. Ghaddar).

https://doi.org/10.1016/j.solener.2019.05.037
Received 22 February 2019; Received in revised form 6 May 2019; Accepted 15 May 2019
Available online 22 May 2019

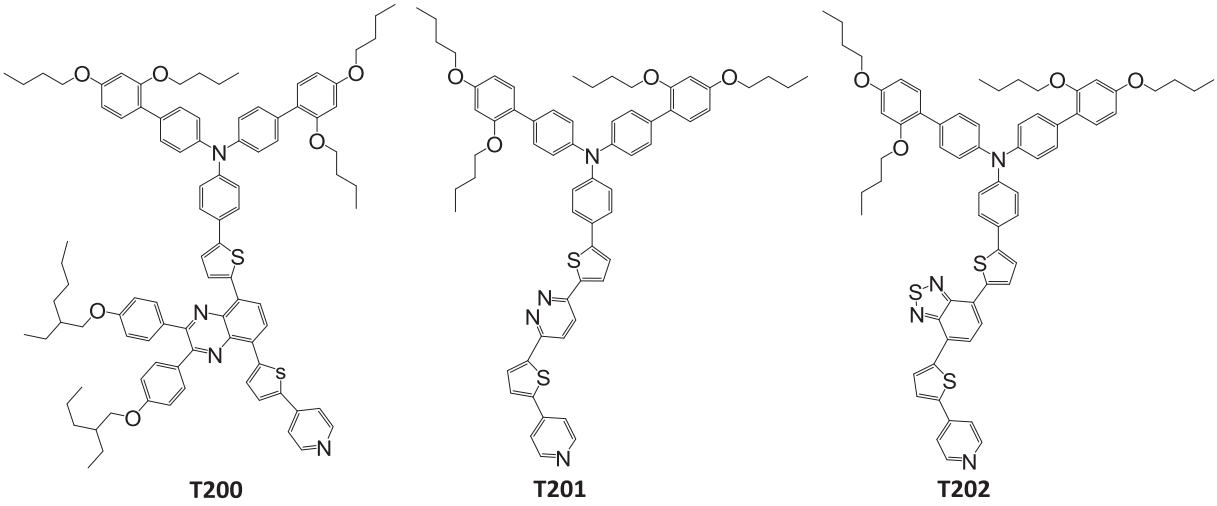

Scheme 1. Molecular structures of the T200, T201, T202, T220, T221 and T222 dyes.

inspired by the fact that these dyes could be used as co-adsorbents with any efficient carboxy-based dyes that possess complementary absorption spectra in order to enhance their DSSCs' short-circuit currents (J_{SC}). In addition, upon co-sensitization we expect a higher surface coverage of the titania film which would result in blockage of electron recombination pathways thus resulting in higher open-circuit photovoltage (V_{oc}); all of which would result in higher DSSCs' efficiencies (Pazoki et al., 2014).

2. Results and discussion

The yellow to turquoise dyes, Scheme 1 and Fig. S1, were synthesized via a Suzuki coupling reaction where the linking of the triphenylamine donor group and pyridine anchoring group to the middle acceptor unit was accomplished simultaneously in one-pot synthesis (Scheme S1).

The absorption spectra of the dyes in THF are demonstrated in Fig. 1, and the corresponding data are listed in Table 1 in addition to the emission maxima. Absorption maxima of 502, 432, 520, 434, 624 and 670 nm with the corresponding molar absorptivities (ε) of 3.1×10^4, 5.2×10^4, 4.3×10^4, 4.0×10^4, 4.8×10^4 and $1.7 \times 10^4\ M^{-1}\ cm^{-1}$ for T200, T201, T202, T220, T221 and T222 were attained, respectively. Differential pulse voltammetry (DPV) was used to measure the first oxidation potentials (E_{ox}) of the dyes in DMF

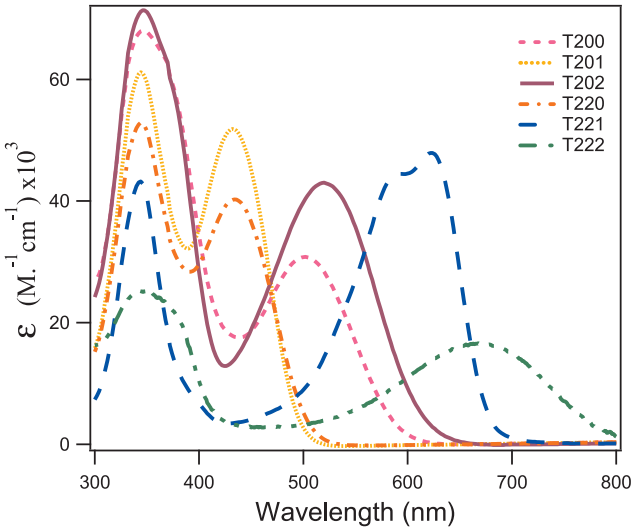

Fig. 1. Absorption spectra of T200 to T222 in THF.

Table 1
Optical and electrochemical properties of T200, T201, T202, T220, T221 and T222.

Dye	Abs. ($\varepsilon \times 10^4\,M^{-1}\,cm^{-1}$)[a]	λ_{em}, nm	E_{ox}, V vs NHE[b]	$E_{ox} - E_{0\text{-}0}$ V vs NHE
T200	346 (6.8), 502 (3.1)	682	1.04	−1.07
T201	344 (6.1), 432 (5.2)	565	1.07	−1.44
T202	350 (7.1), 520 (4.3)	705	1.05	−1.08
T220	344 (5.3), 434 (4.0)	570	1.07	−1.42
T221	342 (4.3), 624 (4.8)	679	1.05	−0.85
T222	347 (2.5), 670 (1.7)	N.D.	0.96	< −0.6

[a] Absorption and emission spectra were measured in THF at 25 °C.
[b] The redox potentials were measured in DMF containing 0.1 M $TBAPF_6$ as supporting electrolyte, a platinum working electrode and an Ag/Ag^+ (calibrated with ferrocene/ferrocenium as an internal standard) as the reference electrode.

solution (refer to Table 1 and Fig. S2). The redox potential of the excited dyes' states, calculated from the redox potential (E_{ox}) and the optical energy gap ($E_{0\text{-}0}$) (measured from the intersection of the absorption and emission bands) by $E_{ox} - E_{0\text{-}0}$ was found to be −1.07, −1.44, −1.08, −1.42, and −0.85 V vs NHE for T200, T201, T202, T220, and T221, respectively. These values are more negative than the TiO_2 conduction band edge (−0.5 V vs. NHE) suggesting an efficient and fast electron injection into the semiconductor. In the case of T222, we estimated the $E_{ox} - E_{0\text{-}0}$ to be less than −0.6 V vs. NHE, which is barely above the CB of TiO_2.

The performance of the six dyes in fully functional DSSCs was evaluated by fabricating cobalt-based DSSC devices whereby the *I-V* curves measured under standard AM 1.5 Global conditions and are shown in Fig. 2. The corresponding photovoltaic parameters are summarized in Table 2. The DSSC based on T202 as a sensitizer showed the highest photovoltaic performance with a $J_{sc} = 13.4\,mA\,cm^{-2}$, a $V_{oc} = 823$ mV, a fill factor *FF* of 0.61, and an overall efficiency PCE% of 6.8%. T222 showed the poorest performance with a PCE% of 0.1%, a short-circuit current of 0.3 $mA\,cm^{-2}$, an open circuit voltage of 498 mV and a fill factor of 0.47. Mediocre values were obtained for T201, T220 and T221 having a J_{sc} of 8.0, 6.1 and 6.7 $mA\,cm^{-2}$, a V_{oc} of 828, 773 and 669 mV, a *FF* of 0.61, 0.68 and 0.60 and finally PCE's% of 4.0, 3.3 and 2.7%, respectively. An overall PCE% value of 5.4% ($J_{sc} = 11.8\,mA\,cm^{-2}$, $V_{oc} = 751$ mV, $FF = 0.61$) was obtained for a DSSC using T200.

Action spectra of monochromatic incident to photon current

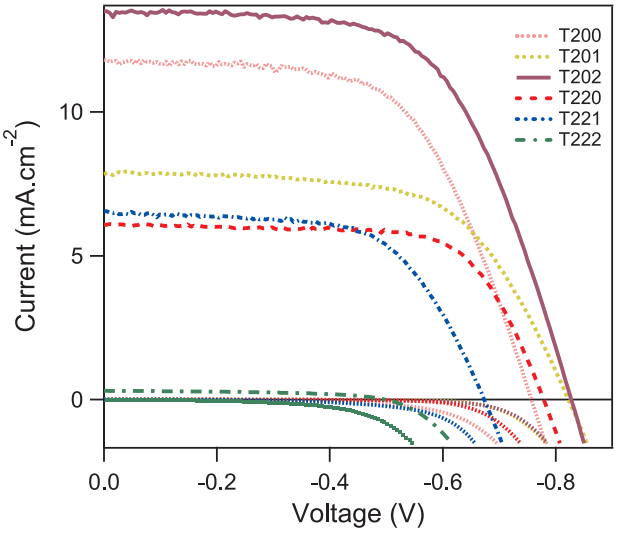

Fig. 2. Photocurrent–voltage characteristics of DSSCs sensitized with T200, T201, T202, T220, T221 and T222 and the corresponding dark currents.

Table 2
Photovoltaic properties of T200, T201, T202, T220, T221 and T222.

Dye	J_{sc}, mA cm^{-2}	V_{oc}, mV	*FF*	PCE (%)[a]
T200	11.8	751	0.61	5.4
T201	8.0	828	0.61	4.0
T202	13.4	823	0.61	6.8
T220	6.1	773	0.68	3.3
T221	6.7	669	0.60	2.7
T222	0.3	498	0.47	0.1[b]

[a] Measured under 100 mW cm^{-2} simulated AM1.5 spectrum with an active area 0.5 × 0.5 cm and a black mask (0.6 × 0.6 cm); the electrolyte consisted of 0.25 M Co(II), 0.06 M Co(III), 0.1 M $LiClO_4$ and 0.6 M TBP.
[b] 0.2 M TBP.

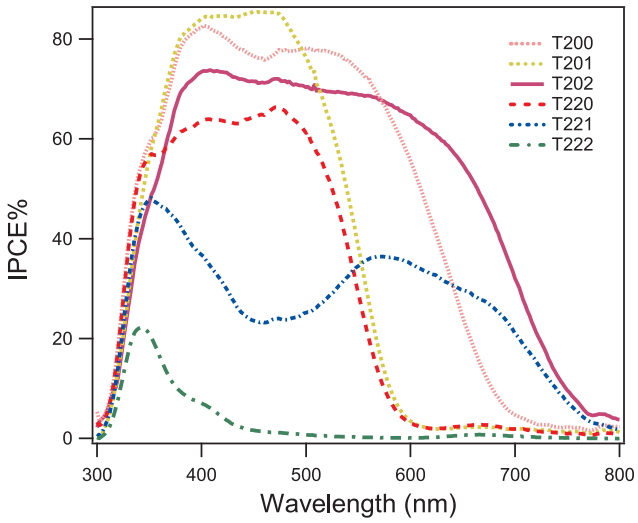

Fig. 3. IPCE% spectra of DSSCs sensitized with T200, T201, T202, T220, T221 and T222.

efficiency (IPCE%) for the six DSSCs are shown in Fig. 3. The onset wavelength of the IPCE spectrum for the DSSC based on T201 was 610 nm, similar to that of T220, however, IPCE values of around 65% were recorded for T220 whereas values up to 85% were observed for T201 in the range of 350–550 nm. With a starting wavelength of 770 nm, a maximum of around 72% at 400 nm was observed for T202-based solar cells. With a similar onset wavelength to T202, T221 exhibits a shoulder at around 690 nm, and a maximum of around 47% at 350 nm. T222 demonstrated the lowest IPCE% among all of the six dyes as predicted from its *IV* performance.

In order to get some insight on the different performance of each dye, TD-DFT calculations were undertaken, in addition to having a deeper understanding of the optical and electrochemical properties of the six dyes. The results are gathered in Table 3 and the frontier orbitals of interest and their energies are represented in Figs. S3 and 4, respectively. In the six dyes except T222, the HOMO is delocalized mostly over the donor-π triphenylamine-thiophene moiety and extends to the middle acceptor-π such as in the cases of T200, T202 and T221. However, in the case of T222 the HOMO extends all the way to the pyridine moiety and concentrated over the middle acceptor. Such a shift in electron density in the case of T222 might have a profound effect on the electron recombination from TiO_2 to the oxidized T222 dye, and consequently this could be an additional reason besides its low LUMO level for its bad performance in a DSSC. Except for T220, the LUMO are concentrated in all dyes on the acceptor-π-pyridine moiety which is favorable for electron injection into the valence band of TiO_2. In the case of T220, the LUMO is mainly concentrated on the acceptor and does not extend to the pyridine moiety. In addition, even though the calculated HOMO-LUMO bandgap for T220 is slightly lower than

Table 3
Calculated electronic transitions of T200, T201, T202, T220, T221, and T222.

Dye	TDDFT excitation energies, nm[a]	Oscillator strength	Assignment
T200	460.9	1.4714	HOMO → LUMO (56%), HOMO − 1 → LUMO (35%)
T201	407.7	2.2502	HOMO → LUMO (49%), HOMO − 1 → LUMO (26%), HOMO → LUMO + 1 (11%)
T202	521.4	1.4326	HOMO → LUMO (57%), HOMO − 1 → LUMO (37%)
T220	454.1	0.9364	HOMO → LUMO (35%), HOMO − 1 → LUMO (22%), HOMO → LUMO + 1 (22%), HOMO − 1 → LUMO + 1 (10%)
	438.2	1.1820	HOMO → LUMO + 1 (34%), HOMO → LUMO (18%), HOMO − 1 → LUMO + 1 (17%), HOMO − 1 → LUMO (15%)
T221	575.4	1.7170	HOMO → LUMO (74%), HOMO − 1 → LUMO (21%)
	404.7	0.2867	HOMO − 1 → LUMO (54%), HOMO → LUMO + 1 (13%), HOMO → LUMO (10%), HOMO − 3 → LUMO (10%)
T222	708.3	1.6737	HOMO → LUMO (87%), HOMO − 1 → LUMO (10%)
	449.3	0.0854	HOMO − 1 → LUMO (31%), HOMO − 4 → LUMO (29%), HOMO − 3 → LUMO (20%), HOMO − 8 → LUMO (6%)
	413.1	0.3803	HOMO − 1 → LUMO (37%), HOMO − 4 → LUMO (25%), HOMO − 8 → LUMO (15%), HOMO → LUMO (5%)

[a] Only bands with oscillator strength f ≥ 0.02 and wavelengths above 400 nm are listed.

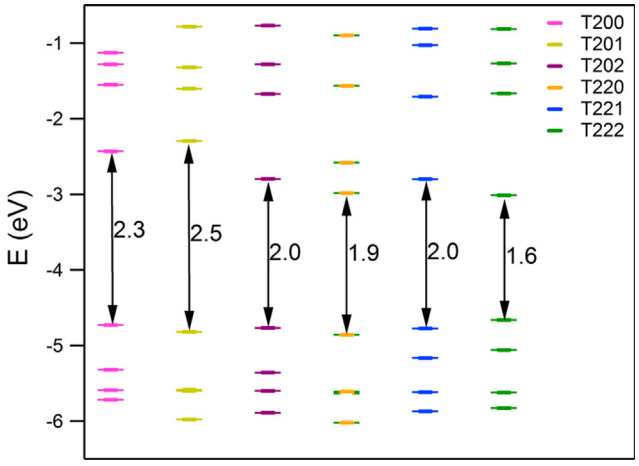

Fig. 4. Calculated energy level diagram of T200, T201, T202, T220, T221, and T222.

that of T202, Fig. 4, the lowest calculated electronic transition is at higher energy than that of T202, Table 3. This latter finding is in good agreement with the experimental absorption spectra and is also mirrored in the calculated assignment of the lowest energy electronic transitions (454 and 438 nm), whereby these transitions are mainly from the HOMO to LUMO + 1 and HOMO − 1 to LUMO levels. Lastly, the calculated absorption spectra for all dyes reproduce quite well the experimental data, where the computed λ_{abs} values follow the experimental absorption maxima.

For the co-sensitization experiments, we selected the T220 dye and co-sensitized it with the commercially available Dyenamo Blue (DB) dye (Hao et al., 2016). The selection of the DB dye was purely based on matching its absorption with that of T220. To begin with, absorbance measurements of the sensitized and co-sensitized films were performed, in addition to measuring the absorption of the corresponding desorbed solutions of the three titania films. Three TiO_2 films with 4 μm thickness were immersed in 0.2 mM solution of T220, 0.03 mM solution of DB, and T220 with DB with the same concentrations in a THF: t-butanol: acetonitrile (1:1:1) mixture for 24 h. The absorption spectra of the dyes attached to the TiO_2 films are shown in Fig. 5A. Next, the desorption of the dye sensitizers from the loaded TiO_2 electrodes was performed, where the individual T220 and BD as well as the co-sensitized T220-BD TiO_2 films were dipped in an alkaline KOH solution with a mixture of THF: ethanol: water. In order to determine the dyes' loading amount of the sensitizers, the absorption spectra of the desorbed solutions were measured, followed by the fitting of the co-sensitized spectrum as shown in Fig. 5B. The dye loading measurements are summarized in Table 4.

Compared to the individually sensitized films, the relative amounts of adsorbed T220 and BD in the co-sensitized film were found to be 88% and 63%, respectively. Ideally these values should be around 100% for both dyes since the anchoring sites are of different nature on TiO_2, however, a very important factor is of relevance here; which is the respective sizes of each dye and its footprint on TiO_2 (Hilal et al., 2018; Su et al., 2017). In the case of T220 and DB, both dyes have very similar calculated vertical distances. In T220 the distance between the nitrogen atoms of the donor and pyridine is 19.8 Å, and in the case of DB the distance between the triphenylamine nitrogen atom and the carboxylic acid anchoring group is 24.3 Å, Scheme 2. As can be seen in Scheme 2, the bulky donor groups of T220 and DB would cause some steric effects, and consequently co-adsorbing of these 2 dyes would result in a decrease in the theoretical total dye loading on the TiO_2 film due to the formation of "dead space" with no adsorbed molecules between the two dyes.

Fig. 6 shows the *IV* and IPCE% curves of the individual and the co-sensitized DSSCs and the data is presented in Table 5. The individually sensitized DB cell exhibits better photovoltaic performance parameters compared to the individual T220 one. The greater difference in the J_{SC} values (J_{SC} = 10.9 and 6.7 mA cm^{-2} for BD and T220, respectively) is due to the fact that T220's absorption is limited to the blue part of the visible region as can also be seen from the IPCE% curve in Fig. 6B. Upon co-sensitization, the T220-DB based device showed notable improvement in the open circuit voltage and the photocurrent, as well as an increase in the power conversion efficiency. The T220-DB co-sensitized device showed an increase in the V_{OC} by 49 mV when compared to DB alone which is also seen in the dark currents where the co-sensitized system exhibits a lower dark current with respect to the individual devices. Furthermore, the increase in J_{SC} for the co-sensitized cell (11.1 mA cm^{-2}) is probably due to the matching of the absorption spectra of T220 and DB as this is also mirrored in the respective IPCE% spectra where it is remarkably broad and covers the whole visible region, which is consistent with the absorption spectra of the co-adsorbed dyes on the TiO_2 film shown in Fig. 5A.

In order to investigate in depth the above mentioned reasoning, electrochemical impedance spectroscopy (EIS) measurements were performed on the three different assembled cells at V_{oc} under different white-light intensity. Fig. 7A and 7B show plots of the charge recombination resistance (R_{CT}) values at the TiO_2/electrolyte interface and the chemical capacitance ($C\mu$), respectively, versus the applied voltage ($_nE_F - E_{F,redox}$), where $_nE_F$ is the electron quasi-Fermi energy level in the TiO_2 film and $E_{F,redox}$ is the electrolyte redox Fermi level. As can been seen from Fig. 7A, the R_{CT} of the T220-DB cell is 10 times higher than that of the single-dye cells. This suggests a lower electron recombination in the co-sensitized T220-DB cell, and this is probably due to the blockage of the cobalt electrolyte from reaching the titania film. This effect is most probably due to the close arrangement of the two dyes in the T220-DB cell, where the alkoxy arms on the donor groups would retard the approach of the Co(III) ions in the electrolyte to TiO_2. As for the $C\mu$ values in the three cells, there wasn't much difference especially when we compare the DB and T220-DB cell, Fig. 7B. Therefore, the longer electron lifetime (τ_n evaluated from the EIS experiments $\tau_n = R_{ct}C_\mu$) of the T220-DB cell is mainly a consequence of its

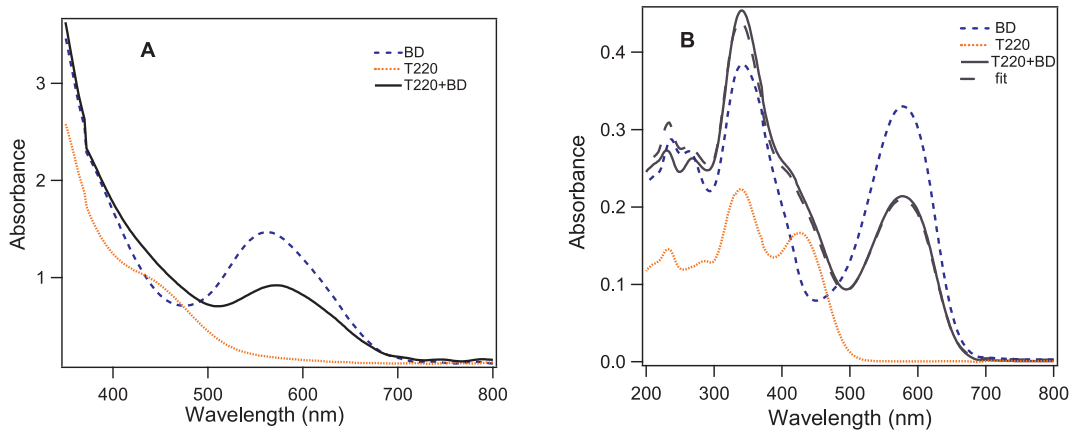

Fig. 5. Absorption spectra of (A) T220, BD, and T220-BD anchored on a 4 μm TiO_2 film and (B) absorbance of the desorbed films of the individual T220 and DB and the co-sensitized T220-DB.

Table 4
Dye loading measurements of the individual and co-sensitized TiO_2 films.[a]

Dye bath concentrations	n_{T220} (moles)	n_{DB} (moles)	Total dye loading (moles)
T220 (0.2 mM)	4.2×10^{-8}	–	4.2×10^{-8}
DB (0.03 mM)	–	6.7×10^{-8}	6.7×10^{-8}
T220 (0.2 mM) + DB (0.03 mM)	3.7×10^{-8}	4.2×10^{-8}	7.9×10^{-8}

[a] The TiO_2 film area is 2.56 cm^2. Each measurement was done in duplicates.

high R_{CT}, Fig. 8. Clearly, the higher total dye loading in the T220-DB cell when compared to the individual T220 and DB cells has a positive effect on electron recombination processes, and thus a higher V_{OC} is attained.

3. Conclusions

In summary, we were successful to synthesize six new pyridyl-based dyes (T200, T201, T202, T220, T221 and T222) with light absorption profiles ranging from the blue to the red of the visible spectrum. The performance of these dyes as sensitizers in cobalt-based DSSCs was evaluated, where T202 showed the best performance with efficiencies approaching 7% which is considered a high value for pyridine-based dyes. We were also successful in co-sensitizing the yellow T220 dye with a blue, DB, one. From absorption experiments performed on films and the corresponding desorbed solutions of the co-sensitized and the individual cells, it was clear that these two dyes do not compete over the adsorption sites (Lewis- and Brønsted-acid sites) of TiO_2. However, due to mismatching of their respective geometrical sizes the total dye loading in the co-sensitized cell was not equal to the theoretical sum of the dye amounts measured for the individual devices. Nevertheless, the photovoltaic performance of the co-sensitized T220-DB cell showed

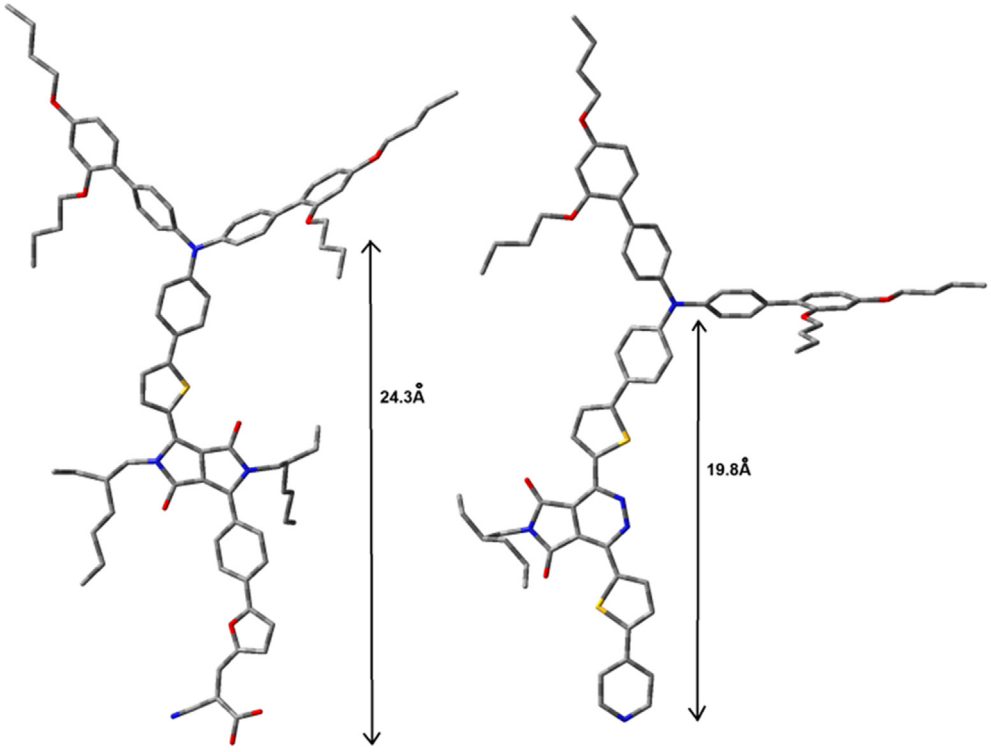

Scheme 2. The calculated vertical distances in T220 and DB dyes.

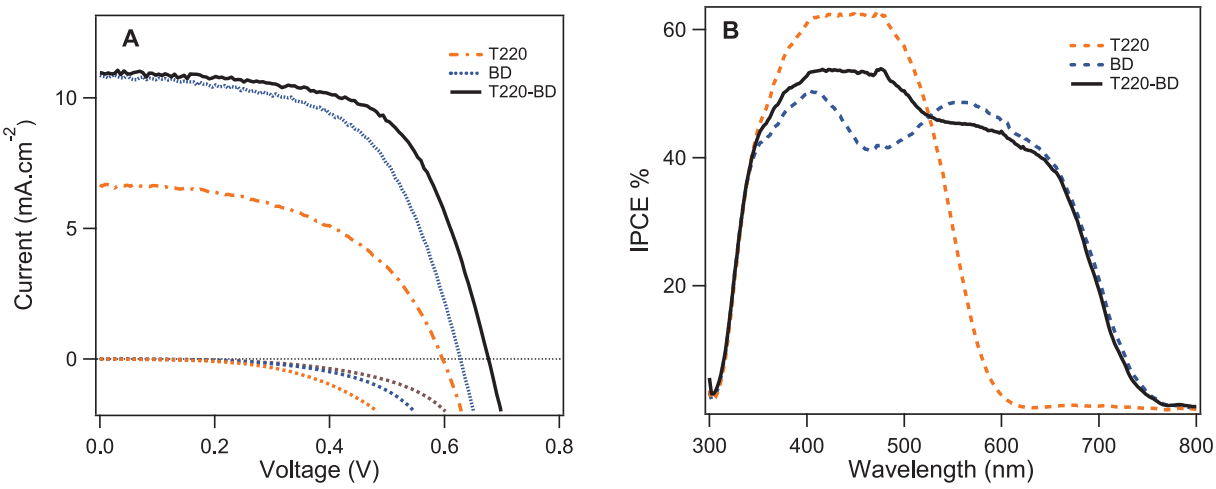

Fig. 6. (A) Photocurrent–voltage characteristics of DSSCs sensitized with the individual T220 and DB dyes and the co-sensitized T220-DB one (B) IPCE% spectra of DSSCs sensitized with the individual T220 and DB dyes and the co-sensitized one T220-DB.

Table 5
Photovoltaic performance of the T220, BD, and co-sensitized T220-DB based devices.[a]

Dye	J_{SC} (mA cm^{-2})	V_{OC} (mV)	*FF*	PCE (%)
T220	6.7	597	0.51	2.04
BD	10.9	625	0.58	3.94
T220-BD	11.1	674	0.54	4.07

[a] The devices were measured under 100 mW cm^{-2} AM 1.5G. 0.25 M Co (II), 0.06 M Co (III), 0.2 M TBP, 0.1 M $LiClO_4$ in acetonitrile.

enhancements in photo-current, photo-voltage and thus total efficiency when compared to the individual T220 and DB cells. The T220-DB cell showed higher open-circuit voltage that was mainly due to the decrease of recombination between the injected electrons into TiO_2 and the cobalt electrolyte, whereby the close packing of the two dyes prevented Co(III) ions from approaching the surface of TiO_2. In addition, this co-sensitization method proved also to have positive effects on the short-circuit currents as demonstrated by the *IV* and IPCE% spectra. Currently, we are working on co-sensitizing the reported dyes with other organic and inorganic dyes, in particular ruthenium based dyes that function very badly with cobalt electrolyte systems due to the very high rates of electron recombination reactions in such devices.

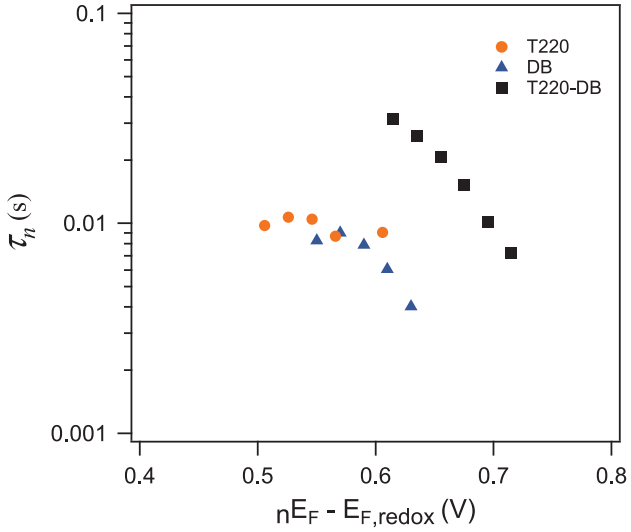

Fig. 8. Electron lifetime values obtained from EIS for the T220, DB and the co-sensitized T220-DB cells.

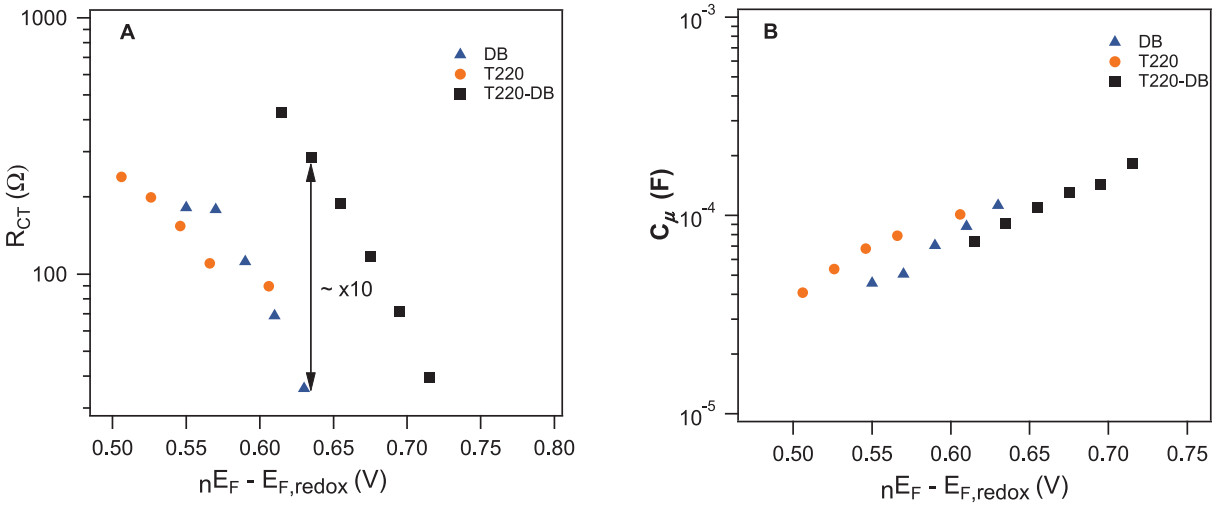

Fig. 7. (A) Charge transfer resistance values obtained from EIS and (B) chemical capacitance values of T220, DB and the co-sensitized T220-DB cells.

Acknowledgments

This work was supported by the University Research Board (Grant 103603) at the American University of Beirut (AUB) and the Lebanese National Council for Scientific Research (Grant 103494).

Appendix A. Supplementary material

Supplementary data to this article can be found online at https://doi.org/10.1016/j.solener.2019.05.037.

References

Ellis, H., Eriksson, S.K., Feldt, S.M., Gabrielsson, E., Lohse, P.W., Lindblad, R., Sun, L., Rensmo, H.k., Boschloo, G., Hagfeldt, A., 2013. Linker unit modification of triphenylamine-based organic dyes for efficient cobalt mediated dye-sensitized solar cells. J. Phys. Chem. C 117 (41), 21029–21036.

Freitag, M., Teuscher, J., Saygili, Y., Zhang, X., Giordano, F., Liska, P., Hua, J., Zakeeruddin, S.M., Moser, J.-E., Grätzel, M., Hagfeldt, A., 2017. Dye-sensitized solar cells for efficient power generation under ambient lighting. Nat. Phot. 11, 372.

Hao, Y., Saygili, Y., Cong, J., Eriksson, A., Yang, W., Zhang, J., Polanski, E., Nonomura, K., Zakeeruddin, S.M., Grätzel, M., Hagfeldt, A., Boschloo, G., 2016. Novel blue organic dye for dye-sensitized solar cells achieving high efficiency in cobalt-based electrolytes and by co-sensitization. ACS Appl. Mat. Interf. 8 (48), 32797–32804.

Harima, Y., Fujita, T., Kano, Y., Imae, I., Komaguchi, K., Ooyama, Y., Ohshita, J., 2013. Lewis-acid sites of TiO2 surface for adsorption of organic dye having pyridyl group as anchoring unit. J. Phys. Chem. C 117 (32), 16364–16370.

Hilal, H.M., El Bitar Nehme, M.A., Ghaddar, T.H., 2018. Large enhancement of dye sensitized solar cell efficiency by co-sensitizing pyridyl- and carboxylic acid-based dyes. ACS Appl. Energy Mater. 1 (6), 2776–2783.

Islam, A., Akhtaruzzaman, M., Chowdhury, T.H., Qin, C., Han, L., Bedja, I.M., Stalder, R., Schanze, K.S., Reynolds, J.R., 2016. Enhanced photovoltaic performances of dye-sensitized solar cells by co-sensitization of benzothiadiazole and squaraine-based dyes. ACS Appl. Mater. Int. 8 (7), 4616–4623.

Joshi, D.N., Ilaiyaraja, P., Sudakar, C., Prasath, R.A., 2018. Facile one-pot synthesis of multi-shaped silver nanoparticles with tunable ultra-broadband absorption for efficient light harvesting in dye-sensitized solar cells. Sol. Energy Mater. Sol. Cells 185, 104–110.

Kakiage, K., Aoyama, Y., Yano, T., Oya, K., Fujisawa, J.-I., Hanaya, M., 2015. Highly-efficient dye-sensitized solar cells with collaborative sensitization by silyl-anchor and carboxy-anchor dyes. Chem. Commun. 51 (88), 15894–15897.

Kuang, D., Walter, P., Nüesch, F., Kim, S., Ko, J., Comte, P., Zakeeruddin, S.M., Nazeeruddin, M.K., Grätzel, M., 2007. Co-sensitization of organic dyes for efficient ionic liquid electrolyte-based dye-sensitized solar cells. Langmuir 23 (22), 10906–10909.

Lodermeyer, F., Costa, R.D., Malig, J., Jux, N., Guldi, D.M., 2016. Benzoporphyrins: selective co-sensitization in dye-sensitized solar cells. Chem. – A Eur. J. 22 (23), 7851–7855.

Mathew, S., Yella, A., Gao, P., Humphry-Baker, R., Curchod, B.F.E., Ashari-Astani, N., Tavernelli, I., Rothlisberger, U., Nazeeruddin, M.K., Grätzel, M., 2014. Dye-sensitized solar cells with 13% efficiency achieved through the molecular engineering of porphyrin sensitizers. Nat. Chem. 6, 242.

O'Regan, B., Grätzel, M., 1991. A low-cost, high-efficiency solar cell based on dye-sensitized colloidal TiO2 films. Nature 353, 737–740.

Pazoki, M., Lohse, P.W., Taghavinia, N., Hagfeldt, A., Boschloo, G., 2014. The effect of dye coverage on the performance of dye-sensitized solar cells with a cobalt-based electrolyte. Phys. Chem. Chem. Phys. 16 (18), 8503–8508.

Su, J., Zhu, S., Chen, R., An, Z., Chen, X., Chen, P., 2017. Study on dye-loading mode on TiO2 films and impact of co-sensitizers on highly efficient co-sensitized solar cells. J. Mater. Sci.: Mater Electron. 28 (5), 3962–3969.

Tsai, M.-C., Wang, C.-L., Chang, C.-W., Hsu, C.-W., Hsiao, Y.-H., Liu, C.-L., Wang, C.-C., Lin, S.-Y., Lin, C.-Y., 2018. A large, ultra-black, efficient and cost-effective dye-sensitized solar module approaching 12% overall efficiency under 1000 lux indoor light. J. Mater. Chem. A.

Yella, A., Lee, H.-W., Tsao, H.N., Yi, C., Chandiran, A.K., Nazeeruddin, M.K., Diau, E.W.-G., Yeh, C.-Y., Zakeeruddin, S.M., Grätzel, M., 2011. Porphyrin-sensitized solar cells with cobalt (II/III)–based redox electrolyte exceed 12 percent efficiency. Science 334 (6056), 629–634.

Yum, J.-H., Jang, S.-R., Walter, P., Geiger, T., Nüesch, F., Kim, S., Ko, J., Grätzel, M., Nazeeruddin, M.K., 2007. Efficient co-sensitization of nanocrystalline TiO2 films by organic sensitizers. Chem. Commun. 44, 4680–4682.

Yun, M.J., Cha, S.I., Seo, S.H., kim, H.S., Lee, D.Y., 2015. Insertion of dye-sensitized solar cells in textiles using a conventional weaving process. Sci. Rep. 5, 11022.